Use of the mark-tracking method for optical fiber characterization

Vichith Chean, Eric Robin, Rochdi El Abdi, Jean-Christophe Sangleboeuf, Patrick Houizot

Use of the mark-tracking method for optical fiber characterization

V. Chean, E. Robin, R. El Abdi *, J-C. Sangleboeuf, P. Houizot

Université de Rennes1, Larmaur, ERL CNRS 6274, Campus de Beaulieu, 35042 Rennes Cedex, France

The mark tracking method was used in the uniaxial tensile test to determine the elastic properties of optical fibers. The mark tracking method is based on the follow up of two markers on the specimen with the help of an image processing technique. It allows us to determine the true strain with respect to the small strains assumption ($\leq 1\%$) or the finite strains ($> 1\%$) without any impact of the rigid solid movement or pulley fiber sliding on the measured strain. Both coated optical fiber and stripped fiber were subjected to the uniaxial tensile test and the cantilever beam bending test. The Young' modulus results of the stripped fiber were found to be very similar for both tests. Thus, the mark tracking method is adaptable to the tensile test of optical fibers and the elastic behaviors of both coated optical fiber and stripped fiber are found to be non linear. Their Young's moduli are 22 and 79 GPa, respectively. These results revealed that those coatings play a mechanical role in fiber elongation.

1. Introduction

Besides signal transmission for telecommunications, fibers are used in an increasing number of devices and the availability of silica fibers enlarges the field of possible applications.

A large group of applications encompasses optical fiber sen sors, remote chemical analysis, thermal measurements and ther mal imaging, reflectometry, optical instrumentation and also laser power delivery [1,2]. Most medical applications of fibers, with their specific requirements, are related to this group. Moreover, optical fiber sensors are widely used in smart materials [3 5], for example, in order to monitor civil engineering structures to assess their durability. In the framework of this study, composite material embedded optical fibers were used in order to improve the use in service of high technology bridges which are made up of composite materials. Therefore, elastic properties have been a major consideration in the application of optical fibers. In order to characterize the elastic properties of optical fibers, both coated fiber and stripped fiber (stripped polymer coating fiber) were subjected to mechanical tests. In this work, cantilever beam bending test and uniaxial beam bending test and uniaxial tensile test were performed to determine the Young' modulus and mechanical behavior of silica optical fiber.

The Young' modulus of stripped fiber is determined by a cantilever beam test. Then, to validate this result some uniaxial tensile tests were performed. The uniaxial tensile test was usually used to characterize the mechanical behavior of optical fiber by many studies [6,7]. In this paper, during the tensile testing, an optical method (mark tracking method) is used to measure fiber elongation instead of using the crosshead machine displacement.

2. Fiber structure, fiber reliability and used fiber

2.1. Fiber structure

An optical fiber is a waveguide: a beam of light launched at one end of an optical fiber travels down the fiber with negligible loss of input light. The optical fiber is made of two transparent materials, most of the time glass for the core and the cladding around this. The cross section of most optical fibers is cylindrical, but other geometries (rectangular, flower shaped, D shaped, honeycomb, etc.) have been developed to address particular needs.

2.2. Fiber reliability

As a general rule, the lifetime of the fiber depends mainly on chemical durability and applied stress. Failure corresponds to breaking, which is known to happen as crack propagation from a surface flaw. Real fibers have surface flaws resulting from proces sing. The initial intrinsic strength of a fiber is related to chemical composition, and ultimately to the energy of the chemical bond. Current values are 4 GPa for silica fibers and less than 1 GPa for fluoride and sulfide fibers. Initial strength decreases with respect to time when the fiber is subjected to stress corrosion, or more

* Corresponding author. IUT de Rennes, 3, Rue du Clos Courtel, B.P. 90422, 35704 Rennes Cedex 7, France. Tel.: +33 2 23 23 41 12; fax: +33 2 23 23 41 12.

E-mail address: relabdi@univ-rennes1.fr (R. El Abdi).

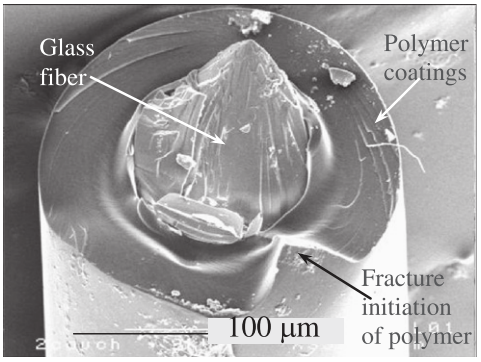

Fig. 1. Silica optical fiber used.

simply, under a permanent stress in a humid environment. This phenomenon has been extensively studied in silica fibers [8].

2.3. Used fiber

In this study, monomode silica optical fibers were used and the fiber diameter is equal to 125 µm. Two acrylate polymer coatings (0.2 NA acrylate coupler fibers) with a thickness of 62.5 µm were used (Fig. 1). The acrylate coating is the most used in standard optical fibers. It protects the fiber but it is not perfectly water tight. The internal layer is soft with a low glass transition temperature (T_g) and is applied onto the glass fiber surface. It ensures protection against micro bending and damping of the external stresses. The external layer has a higher T_g and protects the fiber against physical aggression. To comply with process requirements, UV polymerization of the acrylate resins is rapidly performed, in line, and offers an excellent adhesion and a large range of elasticity (Young's modulus).

Usually, the tensile test is used to determine the Young modulus of a fiber. During a dynamic tensile test, the fiber is subjected to deformation under a constant velocity until rupture. The two fiber ends are rolled up onto pulleys. The lower pulley is fixed while the higher pulley is mobile and its displacement velocity corresponds to the chosen deformation speed to carry out the test. During the test, the deformation and the tensile load are measured using a dynamometric cell while the fiber deformation is deduced from the displacement between the fixed lower pulley and the mobile higher plate. But in some cases, fiber slipping during the dynamic test cannot be prevented and the measured parameters are not exact. In the following study, the mark tracking method is used and leads to correct measurements. The mark tracking method is a non contact technique is well adapted for the measurement of the optical fiber strains. This technique presents great interest: it is not influenced by the motion of the sample, nor sensitive to variation in the sample color and canbe used to analyze both large and small strains.

3. Experimental tests

3.1. Cantilever beam bending test

A cantilever is a beam that is supported only at one end as shown in Fig. 2a. This test, thanks to the strength of materials theory, leads to the determination of the Young' modulus of silica fiber (stripped polymer coated fiber) [9]. The gauge length L of the specimen is 244 mm and stripped fiber density ρ is 2.15 g/cm^3 (measured by helium pycnometry).

The geometry of the bending fiber and the coordinate system that will be used are shown in Fig. 2b. Deflection y along the beam

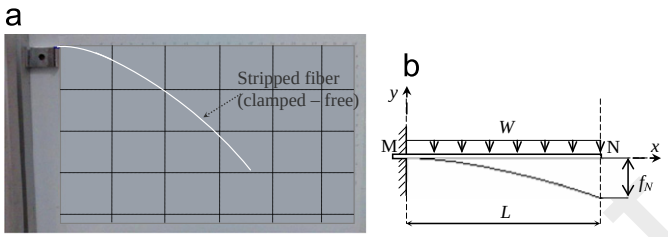

Fig. 2. Cantilever beam test: (a) cantilever beam test of stripped fiber and (b) schema of cantilever.

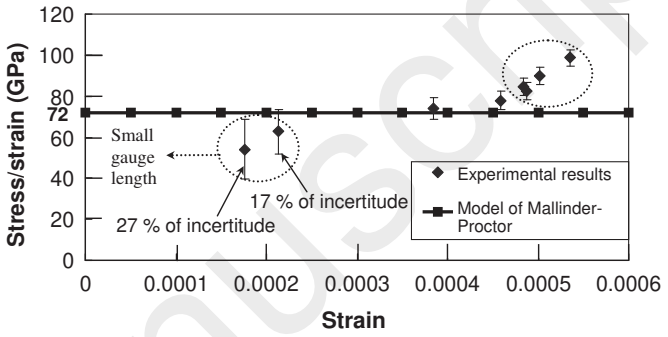

Fig. 3. Comparison with the Mallinder–Proctor model.

is given by

$$y = \frac{Wx^2}{24EI}(x^2 \quad 4Lx + 6L^2) \tag{1}$$

$$I = \frac{\pi d^4}{64} \tag{2}$$

$$W = \rho g \frac{\pi d^2}{4} \tag{3}$$

E and I are, respectively, the Young' modulus and the moment of inertia of the stripped fiber,. W is the self weight load (N/mm), d is the diameter of the stripped fiber equal to 125 µm as measured by optical microscopy and also by SEM (Scanning Electronic Microscopy)and g is the gravity acceleration.

With deflection measured at the free end of the beam, the Young' modulus of a stripped polymer coating fiber is calculated as

$$E = \frac{WL^4}{8f_N I} \tag{4}$$

From Eq. (4), the elastic deflection f_N (in mm) at point N (Fig. 2b) can be obtained:

$$f_N = \frac{WL^4}{8IE} \tag{5}$$

The diameter of the core (wave guide) is 8 ± 1 µm and is positioned on the neutral axis of the beam so that the Young' modulus obtained is that of silica.

The maximum strength σ in the bending section is given by

$$\sigma = \frac{Md}{2I} \tag{6}$$

M is the bending moment at the end support.

The maximum strain ε in the bending section is given by

$$\varepsilon = \frac{\sigma}{E} \tag{7}$$

In this study, eight specimens of different gauge lengths were used in the cantilever bending test.

Fig. 3 gives the σ/εevolution according to ε of experimental results and the theoretical Mallinder Proctor model, which is

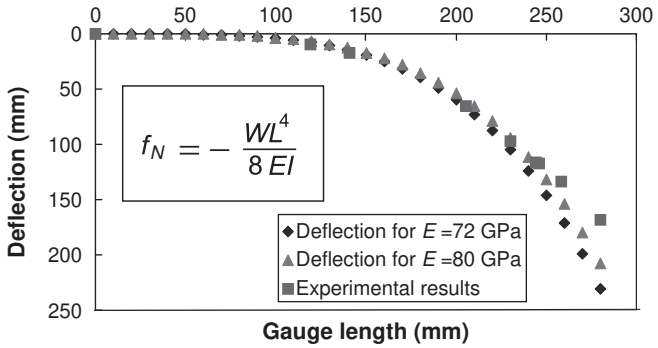

Fig. 4. Deflection versus gauge length for different Young modul.

written as

$$\frac{\sigma}{\varepsilon} = E_0\left(1+\frac{\alpha.\varepsilon}{2}\right) \tag{8}$$

For most silica optical fibers, generally $E_0 = 72$ GPa and $\alpha = 6$ are the chosen values.

For samples with a small gauge length, this can result in a large measurement incertitude (from 17% to 27%) as shown in Fig. 3.

Some experimental results cannot be represented by the Mallinder Proctor model, particularly when $\varepsilon > 0.00049$ (Fig. 3). If only two experimental results ($\varepsilon = 0.00039$ and $\varepsilon = 0.00047$) approach those of the Mallinder Proctor model (Fig. 3), it is not easy to draw a conclusion from the experimental protocol test employed for the fibers used with respect to the strain stress relationship.

On the other hand, using Eq. (5), Fig. 4 gives the evolution of the theoretical deflection f_N for different gauge lengths. Even for a large Young modulus (80 GPa), the experimental results (for gauge lengths greater than 240 mm) cannot be represented by the strength material theory.

We can conclude that the deflection method is not easy to adapt for the optical fiber behavior evaluation and the mechanical fiber behavior cannot be represented by Eq. (5) or by the tradi tional model of Mallinder Proctor.

Therefore, a uniaxial tensile test with the attachment of mark tracking method was chosen to develop a new behavior model.

3.2. Uniaxial tensile test with mark tracking method

3.2.1. Mark tracking method

The mark tracking method is an optical technique that enables local strain computation [10].

The principle of this method consists of tracking marks with the help of image processing. The marks are applied on the fiber specimen with a pencil. During the test, numerical fiber images are stored (the frame rate is 1 image per second).

A digital image is considered as a matrix where each pixel is defined by its position and its intensity. A CCD sensor coded on 8 bits is used and the grey level evolves between 0 and 255. So an algorithm coded in C++ is developed and allows tracking of the marker positions s.

The tracking process is divided into three steps:

- First step
  A zone of interest (ZOI) position is defined. This zone leads to delimiting the image process area of each mark (Fig. 5).
- Second step
  In this step, a calculation area A (in the ZOI) is defined by the operator who chooses a "mask" (a selected zone), where the barycentre calculation will be made. The barycentre

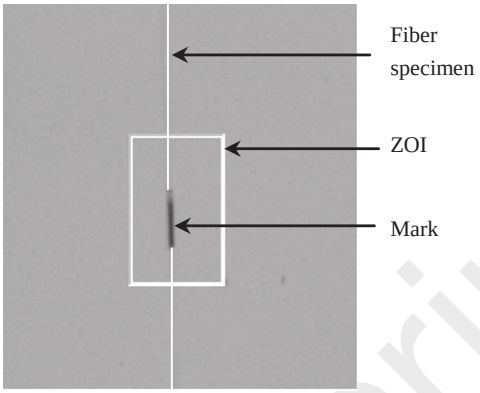

Fig. 5. Zone of interest position (ZOI).

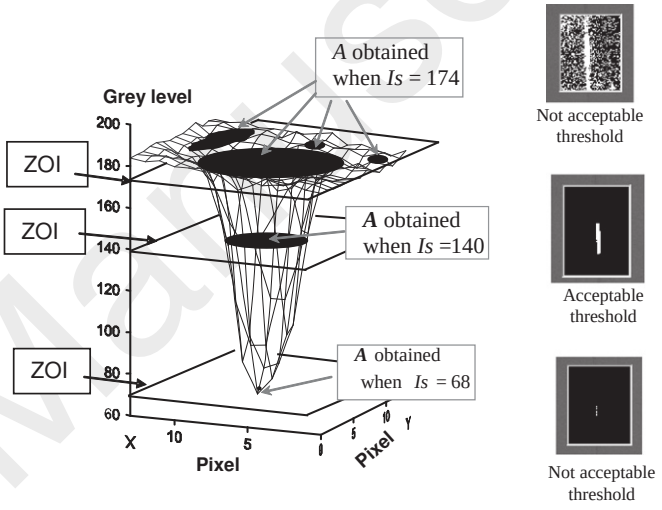

Fig. 6. Evolution of the threshold intensity value.

coordinates are given by [11]

$$\begin{cases} x_g = \dfrac{\sum_i x_i (I_i \quad I_s)}{\sum_i (I_i \quad I_s)} \\ y_g = \dfrac{\sum_i y_i (I_i \quad I_s)}{\sum_i (I_i \quad I_s)} \end{cases} \tag{9}$$

I_i is the grey level of the pixels belonging to A, whose coordinates are (x_i, y_i) and I_s is the threshold value that distinguishes the pixels of markers .Fig. 6 gives a tridimen sional representation of the lower limit of the light intensity I_s. I_s is directly linked to the illumination conditions during the threshold process. One can note (Fig. 6) the influence of I_s on the A calculation area. On the other hand, there must be only one calculation area in the ZOI (due to the process using a barycenter calculation) and the geometrical form of A must not be changed for each acquired image.

As the conditions of the illumination evolve during the test, we cannot use the same value of I_s for each image. An algorithm was developed and allows to recalculation of the optimal I_s value in order to attenuate the illumination variation and to keep the same geometrical form of area A. Indeed, from the optimal value of I_s previously defined by the operator for the first image, the software determines the ratio of $|\text{Max} \quad I_s|$to $|\text{Min} \quad I_s|$. Max and Min represent the grey level optimal values of the image. This ratio helps to recalculate I_s from the optimum grey levels of the next image.

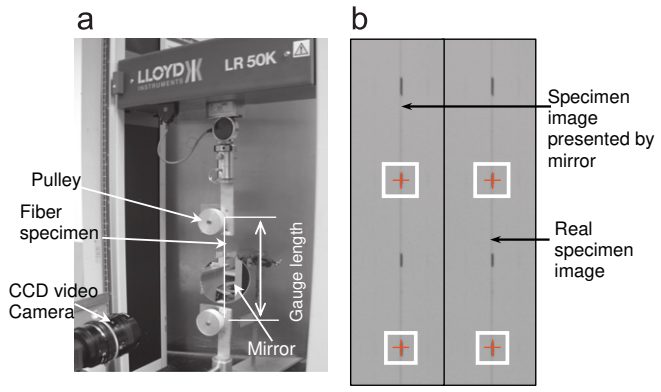

Fig. 7. (a) Data acquisition system devices and (b) Image analysis.

- Third step
  From ZOI position and the I_s value defined by the operator at the first image, the software tracks automatically the marks (the software can simultaneously track four marks) and calculates the mark positions for the next image. Thus, the optimal I_s value is automatically computed for each image and if the barycenter position of mark gets too close to ZOI border, the ZOI position is automatically redefined.

Two markers are gently and carefully deposited in order to avoid incidental surface cracks on the fiber surface, as is the case when permanent marker pen is used. Strain determination was carried out using the principle of measurement.

The calculation of mark position is performed with only one camera and the out of plan fiber position cannot be estimated. The out of plan displacement is prejudicial for the method accuracy, since this phenomenon induces geometrical distortion. Thus, a stereo system is used. A camera with a mirror (which gives another visualization plan) was used (Fig. 7). The out of plan displacement is carefully controlled by using a mirror inclined at 45° with respect to the axis of CCD camera. This set up allows determining the three dimensional position of each mark during the test. When and only when the image of a real specimen and the one of the mirror presented specimen were superimposed (out of plan compound was not detected), the test results were analyzed. Once the marks are located, the length between the two markers $l(t)$ and the strain $\varepsilon(t)$ are calculated every second following the principle of the deformation measurement.

3.2.2. Principle of deformation measurement

In Fig. 8, the line segment M_1M_2, considered as the segment of the two markers at the initial state (time $t=0$) in the reference $(O,\vec{X},\vec{Y})$, changes into the segment M_3M_4 at time t (change is measured every second) once a load is applied.

The deformed length $l(t)$ and the initial length L are given by

$$l(t) = \sqrt{(X_4 \quad X_3)^2 + (Y_4 \quad Y_3)^2} \tag{10}$$

and

$$L = \sqrt{(X_2 \quad X_1)^2 + (Y_2 \quad Y_1)^2} \tag{11}$$

Strain calculations are performed with respect to the small strains assumption (strain $\leq 1\%$) or the finite strains (strain $> 1\%$).

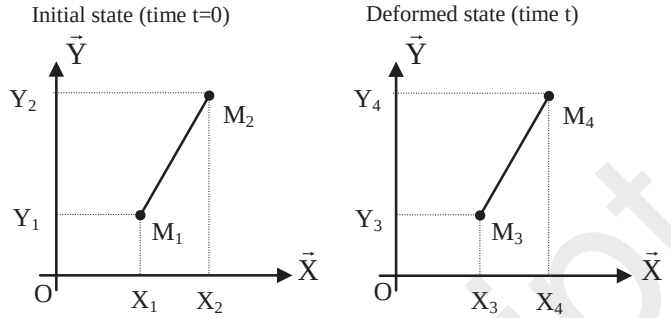

Fig. 8. Deformation of line segment.

For strains greater than 1%, the finite strain assumption is used. Thus, the Euler Almansi finite strain tensor is given by:

$$\varepsilon_{ij} = \frac{1}{2}\left(\frac{\partial u_i}{\partial x_j} + \frac{\partial u_j}{\partial x_i} \quad \frac{\partial u_k}{\partial x_i}\frac{\partial u_k}{\partial x_j}\right) \tag{12}$$

where $\vec{u} = \begin{vmatrix} u_i \\ u_j \end{vmatrix}$ represents the displacement vector.

The uniaxial deformation becomes

$$\varepsilon = \varepsilon_{11} = \frac{1}{2}\left(\frac{[l(t)]^2 \quad L^2}{[l(t)]^2}\right) = \frac{1}{2}\left(1 \quad \left(\frac{L}{l(t)}\right)^2\right) = \frac{1}{2}\left(1 \quad \frac{1}{\lambda^2}\right) \tag{13}$$

If the strains are lower than 1%, the following Equation (14) is used. The engineering normal strain or engineering extensional strain e of the fiber axially loaded is expressed as a change in the length ΔL per unit of the initial length L of the line element or fiber. The normal strain is given by

$$e = \frac{\Delta l}{L} = \frac{l(t) \quad L}{L} = \frac{l(t)}{L} \quad 1 = \lambda(t) \quad 1 \tag{14}$$

λ is a stretch ratio or extension ratio and is defined as the ratio of the final length $l(t)$to the initial fiber length L.

The parameters which must be determined are the coordinates of M_1, M_2 (initial state) and M_3, M_4 (deformed state). Then, one calculates the axial strains of the fiber, which can be small ($\leq 1\%$) or large ($> 1\%$). The tensile strength of the optical fiber σ is calculated as follows:

$$\sigma = \frac{F}{A} \tag{15}$$

where: F is the measured force, A is the cross sectional area of the optical fiber for polymer coated fiber testing or cross sectional area of the glass fiber for stripped polymer coating fiber.

3.2.3. Mark tracking metrology performance

The mark tracking method performance is limited by several sensibilities of parameters such as the light intensity during the test. To study the method accuracy, repeatability tests were done. The tests consist in tracking a mark on a fiber fixed before loading. The change of the barycentre coordinates x_g and y_g is studied and leads to computation of the standard deviation, which gives the method accuracy (Fig. 9). With a small strain assumption ($L \gg l(t) \quad L$) and using Eq. (14), the accuracy formula is

$$\frac{\Delta e}{e} = \frac{\Delta l(t) + \Delta L}{l(t) \quad L} + \frac{\Delta L}{L} \approx \frac{\Delta l(t) + \Delta L}{l(t) \quad L} \Rightarrow \Delta e = \frac{\Delta l(t)}{L} + \frac{\Delta L}{L} = \frac{2\Delta l(t)}{L} \tag{16}$$

The minimum value of L is equal to 150 pixels and the maximum accuracy value of $\Delta l(t)$ is equal to 0.1 pixel. So, the strain accuracy is equal to:

$$\Delta e = \pm 2 \times 0.1/150 = \pm 13 \times 10^{-4} \tag{17}$$

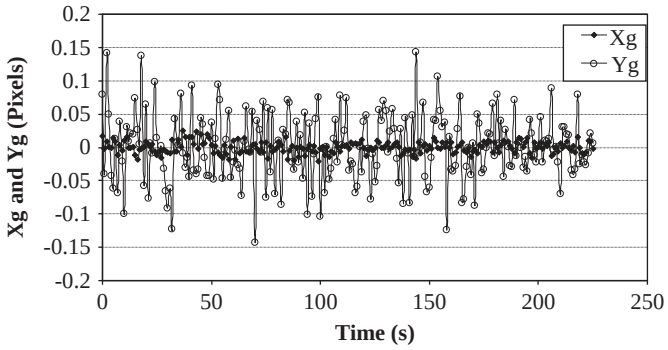

Fig. 9. Evolution of barycentre coordinates during the repeatability test.

3.2.4. Tensile tests

The monitor is used to control the fiber deformation during the test. Recording of marker positions is carried out using a CCD video camera sensor and a data acquisition card. Then all data information is stored in a computer for strain calculations, with corresponding tensile force data for stress calculations. Optical fibers are wound around the pulleys to perform the tensile test as shown in Fig. 7.

The gauge length is 0.2 m and the tests are performed at room temperature (19 ± 1 °C, 40 50% RH). The cross head speeds are 8 and 4 mm/min for polymer coated fiber and stripped polymer coating fiber, respectively. In order to avoid the fibers slipping and damaging the contact area, a double sided tap is applied on the side surface of each pulley on which three windings of the fiber specimen are carried out. For the stripped polymer coating fiber specimen, the stripped length is 2 3 cm in the middle part of the specimen (polymer coated fiber).

4. Experimental results

4.1. Discussion

The main purposes of these tensile tests are to find out Young's modulus of used polymer coated fiber (PCF) and stripped fiber (SF), and to analyze the mechanical fiber behavior.

Results from the mirror (Fig. 7b) show that during the tensile tests, no out of plane angle is noticed (the real specimen image and the image presented by the mirror are parallel and the marked points are at the same level) and the strain curves of the real specimen and of the mirror presented specimen are superimposed (Fig. 10). As a result, the mark tracking method is available.

Tables 1 and 2 reveal that Young modul of the polymer coated fiber (PCF) and the stripped fiber (SF) are found to be 22 and 82 GPa with (at first sight) an elastic linear behavior in terms of 5 6% and 3%, deformation respectively as shown in Fig. 11.

In our studies, Young's modulus of silica fibers are found to be around 82 GPa, which is different from the results mentioned in previous studies ($E=72$ GPa) and with a linear stress strain relationship as shown in Fig. 11. Moreover, the stress strain relationship of optical fibers was first examined by Mallinder and Proctor [12] and later by Glaesemann et al. [13]. They found that the relation between stress and strain of an optical fiber is nonlinear. Then, the nonlinear behavior was used in the strength measurement of optical fibers in many studies [14 16]. Hence, there are two aspects to be considered and to be discussed.

The first aspect refers to strain calculation. One would com pare the finite strain assumption in our case, with the small assumption strain e. As the strain results varied from 3% to 6%, the

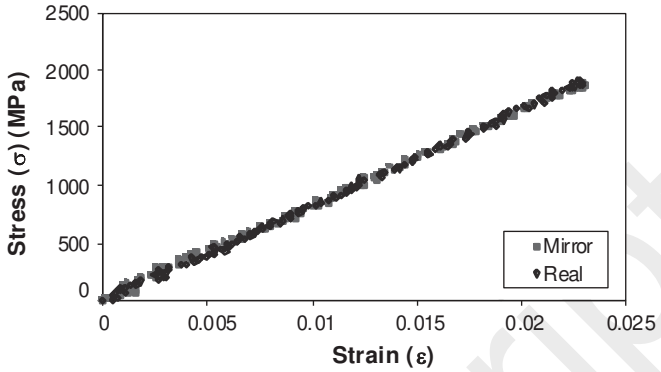

Fig. 10. Results from mirror and real measurements.

Table 1
Mechanical property of polymer coated fiber (PCF).

Sample number	Diameter $\times 10^{3}$(mm)	Failure strain (%)	Young's modulus (GPa)
1	245	5.4	21.96
2	245	5.3	23.13
3	245	5.3	22.11
4	245	5.0	22.02
		Average	22.30
		Standard deviation	0.55

Table 2
Mechanical property of stripped fiber (SF).

Sample number	Diameter $\times 10^{3}$(mm)	Failure strain (%)	Young's modulus (GPa)
1	125	2.3	81.92
2	125	2.5	81.12
3	125	2.7	81.91
4	125	2.2	83.38
5	125	3.0	83.42
		Average	82.35
		Standard deviation	1.01

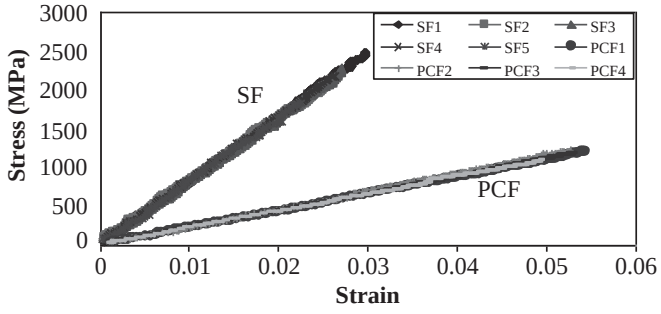

Fig. 11. Stress–strain curve of polymer coated fiber (PCF) and stripped fiber (SF).

strains calculated by the small assumption, e (Eq.(14)), and the finite ones (ε) (Eqs. (12) and (13)) are very similar.

For the five tested samples (SF), the same behavior was seen. Fig. 12 gives for sample No 4 (SF4), the experimental values of σ/ε (σ is calculated using Eq. (15)) according to ε as well as the Mallinder Proctor theoretical model, which is written as

$$\frac{\sigma}{\varepsilon} = E_0\left(1+\frac{\alpha.\varepsilon}{2}\right) \tag{18}$$

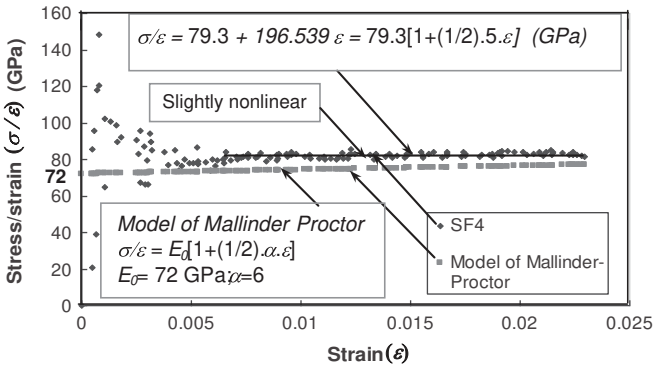

Fig. 12. Nonlinear behavior of used glass fiber.

Non linear fiber behavior actually exists; the experimental values approach the Mallinder Proctor curve. A small dispersion of the experimental values is to be noted for low deformations (at the beginning of the test;$\varepsilon < 0.005$). This may be due to the setting up of the fiber at the beginning of the test and to the complex material behavior for small strain $\varepsilon < 0.005$;Fig. 12).

On the other hand, if the experimental values are interpolated when ε varies between 0.005 and 0.023 ($0.005 < \varepsilon < 0.023$), they can be represented by a non linear function in the form (Fig. 12)

$$\frac{\sigma}{\varepsilon} = 79.3\left(1 + \frac{5.\varepsilon}{2}\right) \tag{19}$$

Thus, a non linear behavior exists for the fiber, although this behavior is slightly non linear for the Verrillon fibers used (Fig. 12). The silica Young modulus E_0 for these fibers approaches 79 GPa, which is different from the Young modulus obtained for failure strains between 0.02 and 0.03 (Table 1). The nonlinearity coefficient α for these fibers is close to 5 (instead of the median value for pure silica proposed by Mallinder ($\alpha = 6$)).

The second aspect refers to the Young's modulus aspect. We found that the Young' modulus E_0 of the stripped fiber is approximately equal to 79 GPa, which seems to be a high value compared to that of fused silica fiber, which is usually about 72 GPa. Optical fibers used for this study are commercial Verrillon single mode silica fibers [17].

Glass fiber (core and cladding) is a composite material. After being drawn at a high temperature (around 1800 °C), the core and the cladding are cooled and thereafter solidified. Core and clad ding have different dilation coefficients; the core dilation coeffi cient is larger than that of the cladding. When the core cools, it cannot contract because the cladding is opposed to this contrac tion. A strained core and a compressed cladding are obtained. During the tensile test, it is necessary to overcome the residual compressive stresses to which the cladding is subjected before submitting the fiber to a positive tensile stress.

Thus the Young modulus of fiber is higher than that of pure silica, which is a homogeneous material.

4.2. SEM observations

We can note that under tensile stress, the fiber breaks at ultimate failure load and several small length fiber pieces, identical to needles, are scattered. When the polymer coated fiber is submitted to the tensile test, the glass fiber sustains most stress because the polymer coating is much softer than the glass fiber. The glass fiber is pulled out from the polymer coating as shown in Fig.1. It can be seen (Fig.1) that the glass fiber broke with an angle of 45°, which is the typical brittle fracture morphology. The fracture initiation of the polymer coating occurred at the right hand side.

The polymer coating and the glass fiber do not have the same tensile resistance and the polymer coating can stretch more than the glass fiber. On the other hand, the critical glass fiber flaw is not at the same cross section as the critical polymer flaw. Thus, the glass fiber is pulled out from the polymer coating when the glass micro crack reaches a critical value.

5. Conclusion

The cantilever beam bending test is an effective test that enables rapid measurement of the Young' modulus of a fiber, but it is not effective for the determination of stress strain relationship. However, the tensile test provides not only the Young' modulus, but also its linearity presented by the stress strain curves. With the attachment of the mark tracking method in the tensile test, we proved that the Young' modul of both the coated and the stripped fibers are different, respectively, about 22 and 79 GPa, with a slightly nonlinear behavior in terms of 5 6% and 3% deformation respectively, which emphasizes the smallest nonlinear effect of the studied optical fibers. The Young' modulus of the stripped fiber is similar when using either the cantilever beam bending test or uniaxial tensile test.

These results highlight the fact that those coatings play a mechanical role in fiber elongation. It is not easy to characterize optical fibers using a traditional tensile test, during which there can be slips and measurement errors. The mark tracking method presents high simplicity, is fast to use leads to the obtaining of a good strain evaluation with accuracy close to $\pm 10^{-3}$ and is finally the potential and available technique for optical fiber mechanical properties measurements.

On the other hand, the mark tracking method can be easily transferred for an industrial application to obtain local small or large strain measurements. One can use all samples where the distance between two marks is higher than 1 mm.

Acknowledgment

The authors express their gratitude to Verrillon, Inc. (North Grafton, MA) for technical assistance and for material support.

References

[1] Kwon IB, Choi MY, Moon H. Strain measurement using fiber optic total reflected extrinsic Fabry-Perot interfometric sensor with a digital signal processing algorithm. Sensors and Actuators A 2004;112:10–7.
[2] Lee B. Review of the present status of optical fiber sensors. Optical Fiber Technology 2003;9:57–79.
[3] Gandhi MV, Thompson BS. Smart materials and structure, 309. Ed. Chapman&Hall; 1992.
[4] Shin CS, Chiang CC. Fatigue damage monitoring in polymeric composite using multiple fiber Bragg gratings. Int. Journal of Fatigue 2006;28:1315–51.
[5] Majumder M, Gangopadhyay TK, Chakraborty AK. Fibre Bragg gratings in structural health monitoring- Present status and applications. Sensors and Actuators A 2008;147:150–64.
[6] Delobelle B, Thiebaud F, Chappelle D, Perreux D, Placet V, Ferrière R. Comptes Rendus des JNC 16-Toulouse, 2009 ; 10, 28 May. France.
[7] Chen C, Chang TH. Fracture mechanics evaluation of optical fibers. Materials Chemistry and Physics 2002;77:110–6.
[8] Matthewson MJ, Kurkjan CR. Environmental effect on the static fatigue of silica optical fiber. Journal of the American Ceramic Society 1988;71:177–83.
[9] Fanchon JL. Guide de mécanique science et technologies industrielles. Editions Nathan 1996:480.
[10] Brémand F, Dupré JC, Lagare A. Etude du comportement des matériaux et des structures. In: Procceeding of the Photomécanique, vol. 95, Cachan-CAMAC, France, 1995.
[11] Rotinat R, Tié Bi R, Valle V, Dupré JC. Three optical procedures for local large-strain measurement. Strain 2001;37(3):89–98.
[12] Mallinder EP, Proctor BA. Static constants of fused silica as a function of large tensile strain. Physics and Chemistry of Glasses 1964;5:91–103.

[13] Glaesemann GS, Gulati ST, Helfinstine JD. The effect of strain and surface composition on Young's modulus of optical fibers. In: Proceedings of optical fiber communication conference, Technical Digest Series, vol. 1. Optical Society of America, Washington, DC, 1988.
[14] Griffioen W. Effect of nonlinear elasticity on measured fatigue data and lifetime estimation of optical fibers. Journal of the American Ceramic Society 1992;75(10):2692–7.
[15] Matthewson MJ. Optical fiber testing techniques. In: Proceedings of the Society of Photo-Optical Instrumentation Engineers, Critical Review Series, vol. CR50, 1994, p. 31–59.
[16] Gupta PK, Kurkjian CR. Intrinsic failure and non-linear elastic behaviour of glasses. Journal of Non-Crystalline Solids 2005;351:2324–8.
[17] Verrillon, Inc., North Grafton, MA, USA.